MIGRATION BEHAVIOUR OF FISSION PRODUCTS IN CANDU FUEL

M. SAIDY[a], R.A. VERRALL[b], J.F. MOURIS[b], I.J. MUIR[a] and W.H. HOCKING[a]

[a]Corrosion and Surface Science Branch
[b]Fuel Development Branch
AECL, Chalk River Laboratories
Chalk River, Ontario, Canada, K0J 1J0

ABSTRACT

A novel out-reactor method has been developed over the past few years for investigating the migration behaviour of fission products in oxide nuclear fuels, which allows the effects of thermal diffusion, radiation damage and local segregation to be independently assessed. Changes in tailored fission-product distributions that have been created in the near-surface region of polished wafers by ion implantation are precisely determined by depth profiling with high-performance secondary ion mass spectrometry (SIMS). This provides a direct measurement of the diffusive spreading of a well-defined source, which has generally been recognized as the only reliable approach for determining diffusion coefficients. Although bombardment with high-energy ions has been successfully used to simulate radiation-induced diffusion, the focus here will be on the effect of thermal diffusion.

1. INTRODUCTION

Segregation of fission products in oxide nuclear fuels is a determining factor for assessing performance and safety throughout the nuclear fuel cycle [1-4]. Overpressure swelling of the fuel element can occur as a result of the release of inert fission gases from the fuel matrix at high burnup. Several volatile fission products, notably iodine, have been implicated in fuel failures caused by stress-corrosion cracking of the Zircaloy sheath [5]. Release of radionuclides from defected fuel elements during reactor operation contributes to activity transport. Accumulation of segregated fission products at the fuel grain boundaries and at the fuel-sheath interface also enhances the potential for release of radioactivity to the environment in the event of an accident and from spent fuel during storage or after disposal [2-4]. Considerable effort has been expended over the past three decades to develop computer codes for predicting fuel performance, but there are still large uncertainties in the experimental data used to calibrate the physical or empirical models.

Migration to the fuel grain boundaries is the first stage, and normally the rate-determining step, in fission-product segregation and release [3]. Three distinct regimes have been recognized for the diffusion of fission products within the fuel matrix during reactor operation [6]. For temperatures below ~1000 K, migration has been shown to be athermal and directly proportional to the fission rate; this radiation-induced diffusion (RID) arises from transient thermal-spike and pressure-gradient effects that occur along fission tracks [7,8]. At higher temperatures, fission products can move by thermally activated jumps between lattice vacancies created by radiation damage—providing radiation-enhanced diffusion (RED) [6,8]. True thermal diffusion (TD), in which both the formation of lattice vacancies and the movement of fission products are thermally controlled, predominates only above ~1700 K [6,9]. Both TD and RED are strongly influenced by the stoichiometry of the fuel matrix, which directly affects the vacancy population [9,10]. If the solubility limit of a particular fission product in the fuel matrix is exceeded, precipitation as microscopic intragranular particles or bubbles can occur. These sites act as effective traps or sinks for that fission product, thereby inhibiting its migration through the fuel matrix, unless they are disrupted by fission spikes (radiation-induced dissolution) [11,12].

Monitoring the release of radiotracers has been the standard method for assessing fission-product migration in nuclear fuels over the past four decades; however, the correct interpretation of such data can be very difficult and results spanning many orders of magnitude have been reported [6,9,10,13-17]. Direct measurement of the diffusive spreading of a concentrated source, such as a deposited film, which is generally recognized as the only reliable approach for determining diffusion coefficients, has been previously applied only to the lattice atoms of the oxide nuclear fuels [14,15,17,18]. Over the past few years, an improved method for investigating the migration behaviour of fission products in CANDU fuels has been developed [19,20]. Changes in tailored fission-product distributions that have been created in the near-surface region of polished wafers by ion implantation are precisely determined by depth profiling with high-performance secondary ion mass spectrometry (SIMS). The impact of temperature, radiation damage and local segregation can be independently assessed. Although bombardment with high-energy ions has been successfully used to simulate radiation-induced diffusion, the focus here will be on the effect of thermal diffusion.

The migration of iodine in UO_2 single crystals as well as polycrystalline ceramic fuel has been evaluated using ion-implanted distributions spanning five orders of magnitude in fluence, although only lower fluence results are reported here. Thermal anneals were normally performed under a suitably reducing atmosphere to preserve a near stoichiometric UO_2 composition [16]. The partial differential equation that represents Fick's second law was numerically solved (using the *Mathematica* software package from Wolfram Research, Champaign, Illinois) to analyze diffusive spreading of the iodine and to determine accurate diffusion coefficients [21]. Sufficient reliable data have now been obtained to provide an Arrhenius relationship for iodine thermal diffusion in fuel, which will be compared with previous findings derived from release measurements [6,13,14,16]. The effects of trapping at defect sites and excess vacancies caused by higher oxygen potential during annealing will be illustrated. Preliminary results from studies of the thermal diffusion of erbium, which is soluble in the uraninite lattice, will also be presented.

2. EXPERIMENTAL PROCEDURES

The experiments reported here were performed on UO_2 single crystals as well as polycrystalline UO_2 wafers ~2 mm thick, which had been sintered to ~97% of the theoretical density, with polygonal, equiaxed grains mainly 5-15 μm in size (fuel-grade ceramic).

Mechanical damage created by polishing one face of each sample to a 0.05 μm finish was removed by annealing at 1500°C in an atmosphere of Ar-4%H_2 [22]. Tailored concentration profiles of stable isotopes of erbium as well as iodine were then introduced into the near-surface region of the polished face by ion implantation. Buried layers, with near-Gaussian distributions of fission products, at mean projected ranges of ~75 nm and ~150 nm, were created by employing ion-implantation energies in the 400 keV to 1.2 MeV range. These layers were initially produced with a pelletron (at Chalk River Laboratories (CRL)) and later with a tandem accelerator (operated by Interface Science Western at the University of Western Ontario (UWO)). In all cases, the focussed ion beam was rastered across the sample to ensure uniform implantation, and the wafers were divided in two, three or four pieces to obtain identical duplicate samples. The implanted-ion fluence was varied over five orders of magnitude—from 10^{11} ions/cm^2 to 10^{16} ions/cm^2 (data for high fluences were presented in an earlier paper [20]).

Diffusive spreading of the ion-implanted fission-product layer was induced by annealing at peak temperatures of up to 1700°C in a high-density alumina tube furnace. The temperature was ramped up and down at a rate of 10°C/min, and was held at the maximum value for 150 min. Because of the exponential dependence of TD on temperature, lattice migration during the ramped portion of the anneal typically made only a minor contribution to the overall diffusive spreading. A type B thermocouple was used to monitor the *in situ* temperature. The oxygen potential within the tube furnace was controlled by a flowing gas mixture of Ar-4%H_2, which normally preserved a stoichiometric UO_2 composition [16].

The distributions of fission products within both diffused and as-implanted samples were measured by depth profiling with a Cameca IMS 6f SIMS instrument, which has been customized for the safe handling of radioactive materials. A double-focussing magnetic-sector mass spectrometer provides high throughput for secondary ions, which are detected with an electron multiplier operated in the single-ion counting mode. The pressure inside the sample chamber was <10^{-9} Torr during the analyses. A Cs^+ primary-ion beam was used to enhance the yield of negative secondary ions when depth profiling iodine (detected as I^-), whereas sputtering with O_2^+ was employed for analysing electropositive fission products (such as Er^+) [23]. The focussed 10 keV Cs^+ beam, with a diameter of ~30 μm and a current of 25-100 nA, was rastered over an area of 250 μm by 250 μm on the sample surface. Secondary ions were efficiently collected, using a 5 kV extraction field, from a smaller region (60-100 μm in size) located in the centre of the sputtered area to minimize crater-edge effects [23]. For the low-fluence iodine implants considered here, sensitivity was optimized by selecting a large secondary-ion energy range (about 45 eV) that spanned the main part of the energy distribution curve [23]. Similarly, the focussed 12.5 keV O_2^+ primary beam, with a diameter of <50 μm and a current of ~250 nA, was also rastered over the same area and secondary ions were again efficiently collected under similar conditions as indicated above. In this case, energy filtering was employed to reduce interference from molecular ions and thereby improve the dynamic range—secondary ions spanning a range of about 45 eV and centred at about 60 eV higher kinetic energy than the peak of the distribution were collected [23].

The depth scale for every sputter profile was subsequently determined by measuring the depth of the sputtered crater using a Tencor Alpha-Step 500 stylus profilometer, which was routinely calibrated against a thin step-height standard (450±3 nm) from VLSI Standards Inc. Significant roughness developed in the bottom of craters sputtered in polycrystalline samples, arising from differences in sputtering rates for the various UO_2 grain orientations [19]. An average crater depth was then derived from a minimum of six line scans recorded across the central region of each crater in two different directions. Because about 100 grains are included in the analysis area, the effects of different grain orientations should be largely averaged out. Depth profiles were always recorded in pairs—one from a diffused sample and the other from its as-implanted duplicate—under identical operating conditions. The concentration scale for the as-implanted sample was determined from the integrated area under the profile and the known implantation fluence [23]. A relative sensitivity factor (RSF) for I^- or Er^+ normalized to a matrix species could then be derived for these analytical conditions [23]. Finally, application of this RSF to the profile for the diffused sample allowed its concentration scale to be calibrated—independent of any loss due to volatilization from the surface. Generally good agreement was obtained using U, UO and UO_2 as the matrix species for the RSF normalization.

3. RESULTS AND DISCUSSION

Thermal diffusion at 1400°C of iodine ion-implanted in a UO_2 single crystal at 440 keV to a fluence of 1×10^{11} ions/cm^2 is illustrated in Figure 1. The maximum iodine concentration at the peak of the as-implanted reference profile (about 1×10^{16} atoms/cm^3) is just below the threshold level previously identified for defect trapping [20]. Duplicate profiles recorded from the as-implanted as well as the annealed samples demonstrate excellent reproducibility, and the latter show clear evidence of iodine migration into the bulk matrix. A simple diffusion analysis, with a constant diffusion coefficient of 1.7×10^{-15} cm^2/s over the entire depth, provided a reasonable fit to the altered distribution (see Introduction). Repeated experiments on polycrystalline UO_2 ion-implanted with iodine to the same fluence and annealed under the same conditions have yielded diffusion coefficients in the range 1.7-3.3$\times10^{-15}$ cm^2/s [20].

The impact of thermal annealing at 1465°C for 120 min on the distribution of iodine ion-implanted in a UO_2 single crystal at 930 keV to a fluence of 1×10^{13} ions/cm^2 is shown in Figure 2. Aside from a slight decrease in the maximum iodine concentration, which is likely due to the effects of RED associated with the original implantation damage [20], there has been little change in the distribution over the main peak. Conversely, diffusive spreading of iodine in the tail of the distribution is quite apparent at concentrations below ~3×10^{16} atoms/cm^3, which is consistent with the threshold for trapping at immobile defect sites (nanobubbles) that was previously inferred from experiments on polycrystalline fuel samples [20]. These results also provide a convincing demonstration that this migration must be due to lattice diffusion (i.e., there are no grain boundaries in the single crystal). Although the spreading in the tail of the distribution in Figure 2 can be fitted with a simplified diffusion analysis, the correct interpretation of these data is not straightforward.

Significant migration of iodine, ion-implanted in polycrystalline UO_2 at 440 keV to a fluence of 1×10^{11} ions/cm^2, resulting from thermal annealing at 1520°C for 150 min is shown in Figure 3. Agreement between the measured and calculated iodine distributions in Figure 3 is quite good over the entire depth profile. In this case, two separate diffusion coefficients were required to achieve an optimum result, but the smaller coefficient used at shallow depths should probably be regarded as just a fitting parameter (possibly representing implantation damage effects [20]). The diffusion coefficient (6.3×10^{-15} cm^2/s) used for depths of greater than 0.075 μm (i.e., over most of the altered distribution) is about double the values derived at 1400°C, which is qualitatively consistent with the expected temperature dependence. More pronounced diffusive spreading of iodine ion-implanted in polycrystalline UO_2 to a low fluence has been observed after annealing at temperatures of 1650°C [20]. This migration also followed the expected square-root dependence on annealing time and could be fitted (except right at the surface) with a single diffusion coefficient [20].

The thermal diffusion coefficients determined for iodine in stoichiometric UO_2 between 1400°C and 1650°C are plotted on an Arrhenius diagram in Figure 4 (one polycrystalline measurement is not shown because it is coincident with the single-crystal result). Diffusion coefficients previously derived from in-reactor measurements of iodine release from polycrystalline UO_2 at 1400°C span two orders of magnitude (from 10^{-15} to 10^{-13} cm^2/s) [6,9,24], but the few data reported for small UO_2 single crystals (also shown on Figure 4) nearly coincide with the present results. This agreement may be partly fortuitous as the in-reactor migration rates reflect the competing influences of trapping and radiation enhancement on diffusion. Post-irradiation measurements of iodine release from polycrystalline UO_2 samples have been performed at temperatures greater than 1400°C; however, the reported D/a^2 values span three orders of magnitude and there is the additional uncertainty of choosing an appropriate radius (a) for the Booth spheres that are included in the analysis of release data [16,24,25].

In-reactor studies have indicated that I, Xe and Kr diffuse at comparable rates throughout the three diffusion regimes (TD, RED and RID) described in the Introduction [6]. Extensive measurements of fission-gas release from irradiated UO_2 fuels have yielded widely varying results [13-15]. Although some of this divergence undoubtedly reflects real effects, such as single-atom diffusion versus trapping, significant problems with release measurements and their interpretation have also been recognized [13-15,17]. The magnitude of the conundrum is captured by the four relations shown graphically in Figure 4 for D_1, D_2, D_3 and D_4, which have been commonly used to represent fission-gas thermal diffusion (where k is the Boltzmann constant and T is the absolute temperature). The first relation (D_1) was derived from early studies of out-reactor anneals of lightly irradiated UO_2 (fission-product concentrations below the trapping threshold) [26], but has subsequently been claimed to closely represent in-reactor measurements taken to a much higher burnup [6]. Based upon a comprehensive review of fission-gas release literature up to 1987, D_2 and D_3 were recommended for the low-concentration and high-concentration limits, respectively [14]. The last relation (D_4) was derived from out-reactor anneals of high-burnup UO_2 fuel [27] and has subsequently been claimed to be appropriate for in-reactor migration in the thermal-diffusion regime [9]. Although the lines for D_1 and D_3 fall within the vicinity of our new data, neither the activation energies nor the frequency factors are optimum; furthermore, the original basis for D_3 (high trapping) does not apply here. A recent theoretical analysis of iodine migration in UO_2 concluded that the controlling process would likely be uranium self-diffusion, in which case the D_4 activation energy would be correct [28]. The values of the activation energy (3.44 eV) and frequency factor (4.75×10^{-5} cm^2/s) obtained from a fit to our data (also shown in Figure 4) differ from all of the published results, although the divergence is least for the D_1 relation.

An extraordinary result obtained by annealing a polycrystalline UO_2 sample, ion-implanted with iodine at 440 keV to a fluence of 1×10^{11} ions/cm^2, for a second time at a temperature of 1500°C for a period of 150 min (previously annealed at 1400°C for 150 min) is displayed in Figure 5. Iodine appears to have migrated deeply into the bulk of the sample with virtually no loss from the surface (equivalent results were obtained from duplicate profiles). Repeated anneals of other samples (up to as many as four times) have never produced comparable behaviour. The plateau in the iodine concentration over depths between about 0.1 μm and 0.7 μm cannot be explained solely on the basis of thermal diffusion. Conversely, a simple diffusion model provided a reasonable fit to the iodine distribution at depths beyond 0.75 μm, with a diffusion coefficient of 3×10^{-13} cm^2/s, which is almost two orders of magnitude larger than would have been predicted from the results above. An elevated oxygen potential at any point during the thermal anneal, sufficient to cause a small degree of hyperstoichiometry and an abundance of uranium lattice vacancies, offers the most plausible explanation for the behaviour observed in Figure 5. Because coulometric titration of the sample after the diffusion experiment did not reveal detectable levels of excess oxygen, this may have been a transient phenomenon. Failure of the tube furnace, used for the thermal anneals, during the next run suggests oxidation of the sample surface resulting from air ingress through an incipient crack.

The rare earth elements are an important family of fission products that have high solubility in the fuel matrix—as lattice substituents for uranium [9]. Simple thermal diffusion of rare earth elements in uraninite at modest concentrations would therefore be expected, without the complications of trapping and release encountered for iodine. The distribution of ^{166}Er ion-implanted in polycrystalline UO_2 at 1230 keV to a fluence of 3.36×10^{12} ions/cm^2 is shown in Figure 6, before and after thermal annealing at 1600°C for 150 min. Surprisingly, the anneal appears to have had the greatest impact on the tail of the distribution, although evidence of erbium migration is apparent throughout the depth profile. Duplicate profiles recorded at other locations on the annealed sample demonstrated excellent reproducibility. The calculated ^{166}Er distribution agrees very well with the measured profile after the thermal anneal. The calculated distribution was obtained using a small diffusion coefficient (8.3×10^{-16} cm^2/s) for $d < 0.4$ μm, a relatively large diffusion coefficient (5.8×10^{-14} cm^2/s) for $d > 0.8$ μm and a smoothly changing value across the transition zone (0.4-0.8 μm). By analogy with the iodine results above, the small diffusion coefficient could be interpreted as being due to trapping and the large diffusion coefficient would then represent the intrinsic diffusion rate. However, as already noted, trapping effects are not expected for rare earth elements at such low concentrations and the smooth diffusive spreading across the peak of the distribution in Figure 6 is not what was observed for iodine above the trapping threshold.

Alternatively, the small diffusion coefficient could represent the intrinsic diffusion rate and the larger coefficient might reflect enhanced migration involving the grain boundaries. This interpretation is now supported by recent experiments on a UO_2 single crystal (equivalent to those shown in Figure 6) that revealed no evidence of enhanced migration of ^{166}Er in the tail of the distribution. The Arrhenius relationship that has been recommended for uranium diffusion in stoichiometric UO_2 predicts a diffusion coefficient of 5.5×10^{-16} cm^2/s at 1600°C [19], which is in good agreement with the value derived from the main part ($d < 0.4$ μm) of the erbium distribution above. A lattice substituent for uranium in UO_2 might reasonably be expected to diffuse at a similar, but not necessarily identical, rate to uranium. Grain-boundary diffusion is generally presumed to be much faster than lattice diffusion, although there are relatively few reliable measurements [29]. Whether the overall migration (as determined by depth profiles) is significantly enhanced depends not only on the relative diffusion rates but also the effective cross-sectional area of the grain boundaries.

4. CONCLUSIONS

The recently developed ion-implantation/SIMS method for investigating the migration behaviour of fission products in oxide nuclear fuels has been further refined and tested. Additional studies of iodine are consistent with previous experiments and preliminary new results have been obtained for erbium. Improvements have also been made in the techniques used to model diffusive spreading. The effects of thermal diffusion, radiation damage and local segregation or trapping can be independently assessed, although quantitative analysis remains difficult if one process does not predominate.

The diffusion coefficients determined for iodine at low concentrations in both single-crystal and polycrystalline UO_2 at 1400°C are in excellent agreement with previous in-reactor measurements on small UO_2 single crystals [6]. This suggests that the impact of trapping on the in-reactor migration rate (at higher fission-product concentrations) has been largely negated by radiation effects. Sufficient reliable data on iodine thermal migration in stoichiometric UO_2 are now available to evaluate published Arrhenius relationships, which predict diffusion coefficients spanning five orders of magnitude. The new data fall near the midrange of the predicted values; however, none of the Arrhenius expressions provide a good fit over the full range of temperatures. Diffusion information derived from fission-product release measurements is clearly very difficult to interpret properly—in the absence of detailed information on the microscopic redistribution, severe complications arising from trapping and radiation damage may not be recognized. Preliminary values of the activation energy (3.44 eV) and frequency factor (4.75×10^{-5} cm^2/s) obtained from a fit to our recent data differ significantly from all of the published results.

A greatly enhanced iodine diffusion rate observed in one experiment has been attributed to excess uranium lattice vacancies caused by an excursion in the oxygen potential during the thermal anneal. It should be feasible to explore this effect on a systematic basis by annealing samples at different elevated oxygen potentials in a controlled fashion.

Preliminary measurements indicate that lattice diffusion of erbium in stoichiometric UO_2 is comparable with uranium self-diffusion, although evidence of a faster diffusion process associated with grain boundaries was also obtained.

5. ACKNOWLEDGEMENTS

The authors would like to thank J.D. Bonnett at CRL and T. Simpson at UWO for performing the ion implantations. Valuable advice from Hj. Matzke throughout this investigation is gratefully acknowledged.

6. REFERENCES

1. H. Kleykamp, "The Chemical State of the Fission Products in Oxide Nuclear Fuels", Journal of Nuclear Materials, 131, 221-246 (1985).
2. J.R. Matthews, "Technological Problems and the Future of Research on the Basic Properties of Actinide Oxides", Journal of the Chemical Society, Faraday Transactions 2, 83, 1271-1285 (1987).
3. J.H. Gittus, J.R. Matthews and P.E. Potter, "Safety Aspects of Fuel Behaviour During Faults and Accidents in Pressurised Water Reactors and in Liquid Sodium Cooled Fast-Breeder Reactors", Journal of Nuclear Materials, 166, 132-159 (1989).
4. L.H. Johnson and D.W. Shoesmith, "Spent Fuel", in "Radioactive Waste Forms for the Future", Edited by W. Lutze and R.C. Ewing, Elsevier Science, Amsterdam, Chapter 11, 635-698 (1988).
5. B. Cox, "Pellet-Clad Interaction (PCI) Failures of Zirconium Alloy Fuel Cladding—A Review", Journal of Nuclear Materials, 172, 249-292 (1990).
6. J.A. Turnbull, C.A. Friskney, J.R. Findlay, F.A. Johnson and A.J. Walter, "The Diffusion Coefficients of Gaseous and Volatile Species During the Irradiation of Uranium Dioxide", Journal of Nuclear Materials, 107, 168–184 (1982).
7. Hj. Matzke, "Radiation Damage in Crystalline Insulators, Oxides and Ceramic Nuclear Fuels", Radiation Effects, 64, 3–33 (1982).
8. H.Wollenberger, V. Naudorf and M.P. Macht, "Radiation-Induced Diffusion in Nuclear Materials", in "Diffusion Processes", Edited by R.P. Agarwala, Elsevier, Amsterdam 201-234 (1992).
9. M. Hirai, J.H. Davies and R. Williamson, "Diffusivities of Fission Gas Species in UO_2 and $(U,Gd)O_2$ Nuclear Fuels During Irradiation", Journal of Nuclear Materials, 226, 238–251 (1995).
10. R.Lindner and Hj. Matzke, "The Diffusion of Xenon-133 in Uranium Oxide of Varying Oxygen Content", Zeitschrift fur Naturforschung, 14a, 582–584 (1959).
11. J.A. Turnbull and R.M. Cornell, "The Re-Solution of Fission-Gas Atoms from Bubbles During the Irradiation of UO_2 at an Elevated Temperature", Journal of Nuclear Materials, 41, 156–160 (1971).
12. H. Blank and Hj. Matzke, "The Effect of Fission Spikes on Fission Gas Re-Solution", Radiation Effects, 17, 57–64 (1973).
13. Hj. Matzke, "Gas Release Mechanisms in UO_2—A Critical Review", Radiation Effects, 53, 219–242 (1980).
14. Hj. Matzke, "Atomic Transport Properties in UO_2 and Mixed Oxides $(U,Pu)O_2$", Journal of the Chemical Society, Faraday Transactions 2, 83, 1121–1142 (1987).

15. Hj. Matzke, "Diffusion Processes in Nuclear Fuels", in "Diffusion Processes", Edited by R.P. Agarwala, Elsevier, Amsterdam, 9-69 (1992).
16. M.A. Mansouri and D.R. Olander, "Fission Product Release from Trace Irradiated UO_{2+x}", Journal of Nuclear Materials, 254, 22–33 (1998).
17. W.H. Hocking, R.A. Verrall, P.G. Lucuta and Hj. Matzke, "Depth-Profiling Studies of Ion-Implanted Cesium and Rubidium in SIMFUEL and Uranium Dioxide", Radiation Effects and Defects in Solids, 125, 299–321 (1995).
18. A.C.S. Sabioni, W.B. Ferraz and F. Millot, "First Study of Uranium Self-Diffusion in UO_2 by SIMS", Journal of Nuclear Materials, 257, 180–184 (1998).
19. W.H. Hocking, R.A. Verrall and S.J. Bushby, "A New Technique to Measure Fission-Product Diffusion Coefficients in UO_2 Fuel", International Atomic Energy Agency Technical Committee Meeting Proceedings, IAEA-TECDOC-1122, 111–118 (1999).
20. W.H. Hocking, R.A. Verrall and I.J. Muir, "Migration Behaviour of Iodine in Nuclear Fuel", Journal of Nuclear Materials, 294, 45–52 (2001).
21. H.S. Carlslaw and J.C. Jaeger, "Conduction of Heat in Solids", Second Edition, Clarendon, Oxford (1959).
22. Hj. Matzke and A. Turos, "Surface Damage in UO_2 Due to Mechanical Polishing and Ion Bombardment", Journal of Nuclear Materials, 114, 349–352 (1983).
23. R.G. Wilson, F.A. Stevie and C.W. Magee, "Secondary Ion Mass Spectrometry: A Practical Handbook for Depth Profiling", Wiley, New York (1989).
24. C.A. Friskney and J.A. Turnbull, "The Characteristics of Fission Gas Release from Uranium Dioxide During Irradiation", Journal of Nuclear Materials, 79, 184–198 (1979).
25. S.G. Prussin, D.R. Olander, W.K. Lau and L. Hansson, "Release of Fission Products (Xe, I, Te, Cs, Mo and Tc) from Polycrystalline UO_2", Journal of Nuclear Materials, 154, 25–37 (1988).
26. D. Davies, G. Long and W.P. Stanaway, "The Emission of Volatile Fission Products from Uranium Dioxide", United Kingdom Atomic Energy Authority Report, AERE-R4342 (1963).
27. K. Une and S. Kashibe, "Fission Gas Release During Post Irradiation Annealing of BWR Fuels", Journal of Nuclear Science and Technology, 27, 1002–1016 (1990).
28. G. Busker, R.W. Grimes and M.R. Bradford, "The Diffusion of Iodine and Caesium in the $UO_{2\pm x}$ Lattice", Journal of Nuclear Materials, 279, 46–50 (2000).
29. D.R. Olander and P. Van Uffelen, "On the Role of Grain Boundary Diffusion in Fission Gas Release", Journal of Nuclear Materials, 288, 137–147 (2001).

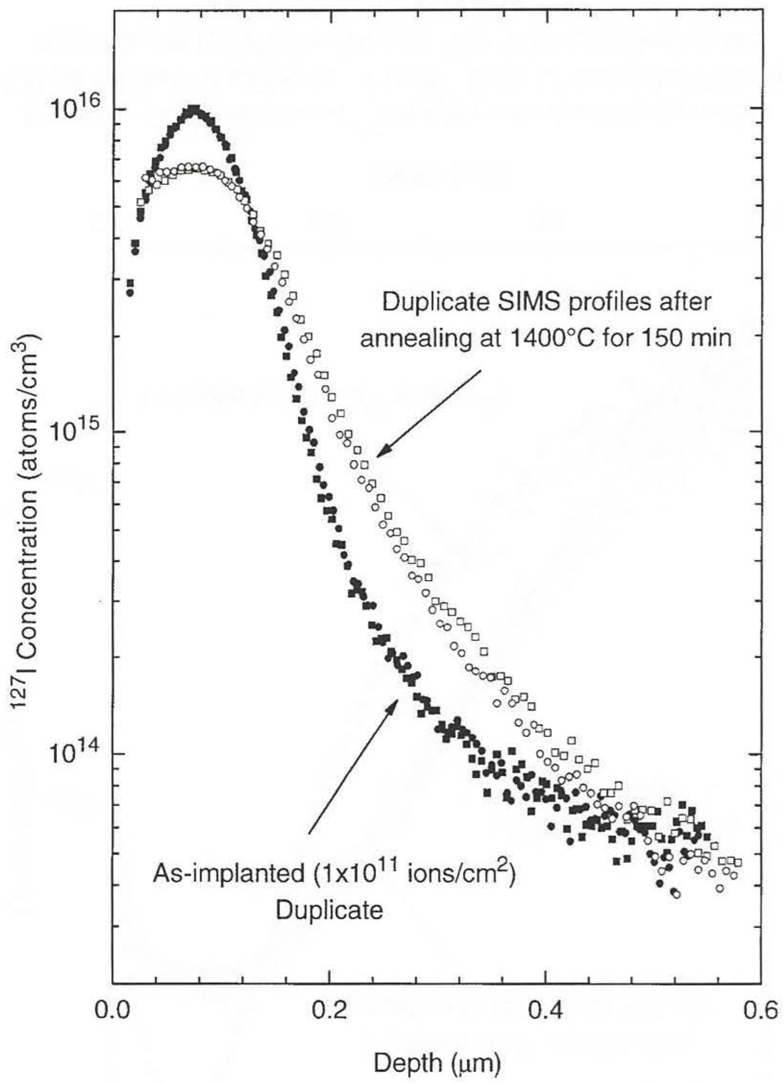

Figure 1. Depth Profiles of ^{127}I As-Implanted in Single Crystal UO_2 at 440 keV to a Fluence of 1×10^{11} ions/cm^2 and After Thermal Annealing at 1400°C for 150 min (Duplicate Profiles Are Shown).

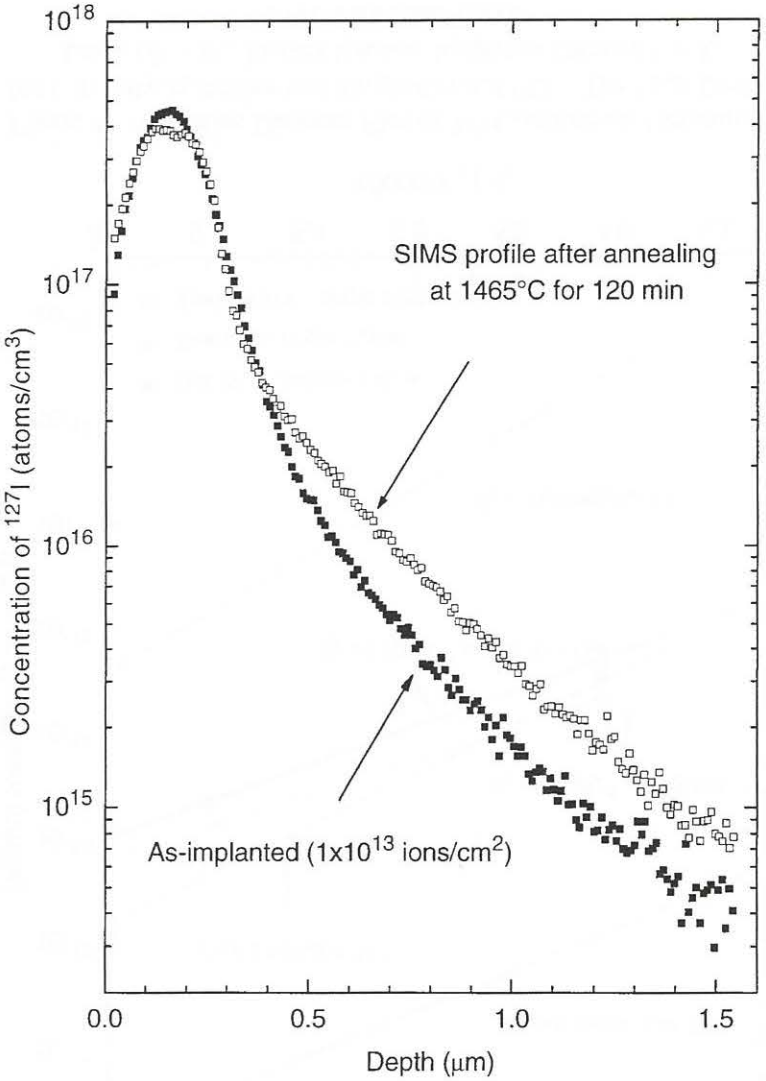

Figure 2. Depth Profiles of ^{127}I As-Implanted in Single Crystal UO_2 at 930 keV to a Fluence of 1×10^{13} ions/cm^2 and After Thermal Annealing at 1465°C for 120 min.

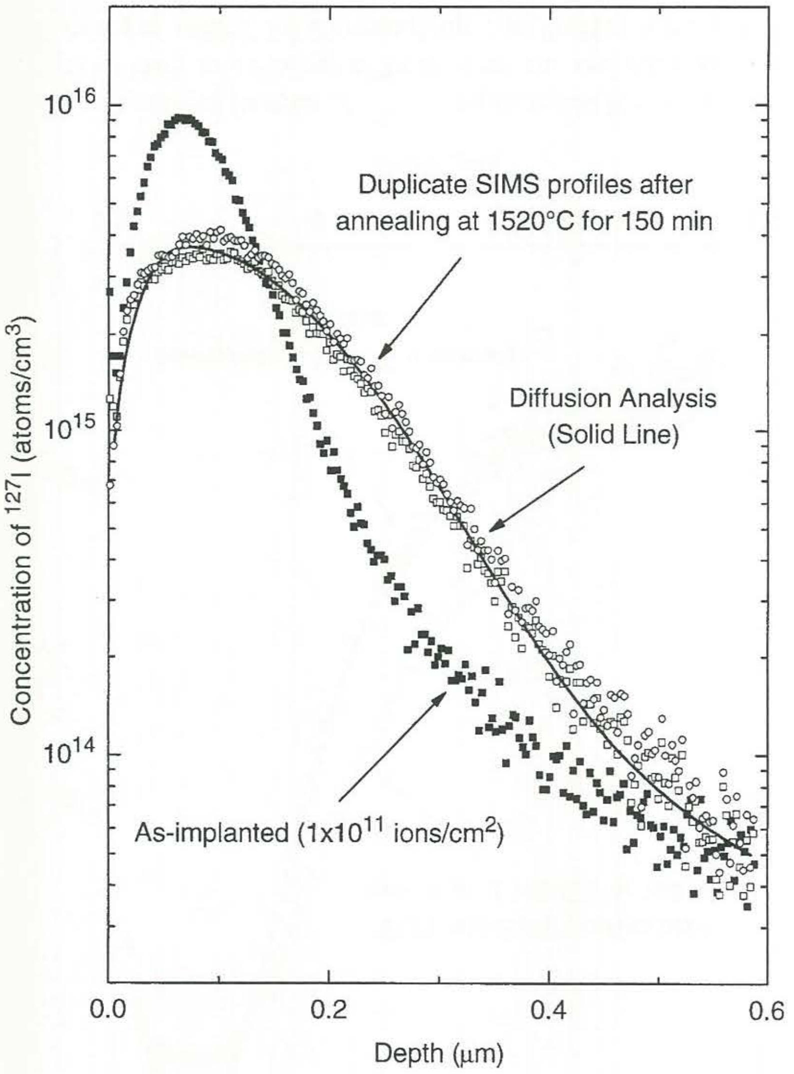

Figure 3. Depth Profiles of ^{127}I As-Implanted in Polycrystalline UO_2 at 440 keV to a Fluence of 1×10^{11} ions/cm^2 and After Thermal Annealing at 1520°C for 150 min. The Solid Line Depicts the Calculated Distribution (See Text).

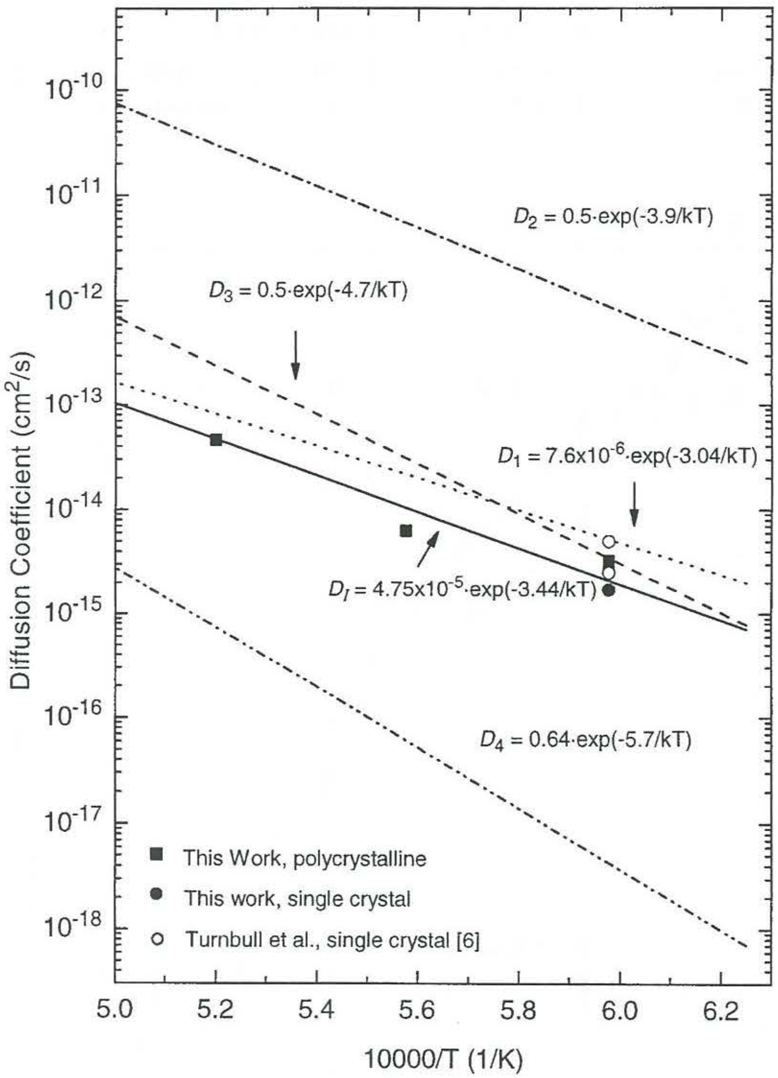

Figure 4. Arrhenius Diagram Plot of TD Coefficients Determined for I in Polycrystalline and Single Crystal UO_2. The Four Broken Lines (D_1 - D_4) Depict Various Relations Derived for Xe Diffusion (See Text).

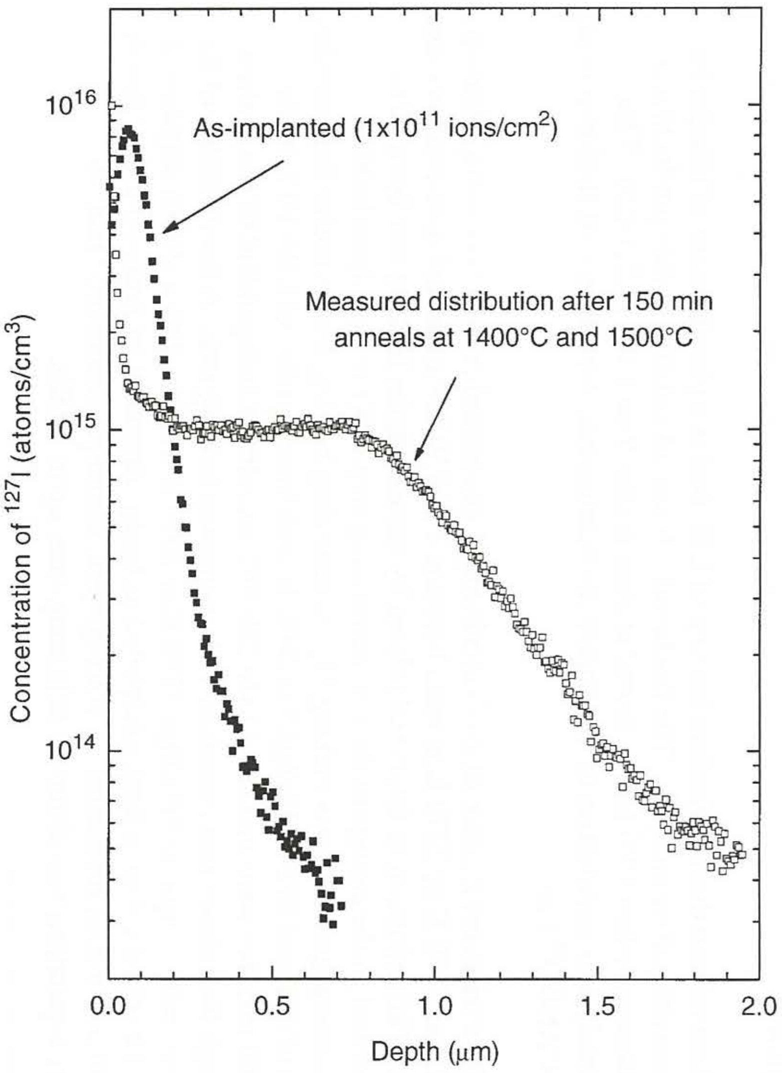

Figure 5. Depth Profiles of ^{127}I As-Implanted in Polycrystalline UO_2 at 440 keV to a Fluence of $1x10^{11}$ ions/cm^2 and After 150 min Thermal Anneals at 1400°C and 1500°C.

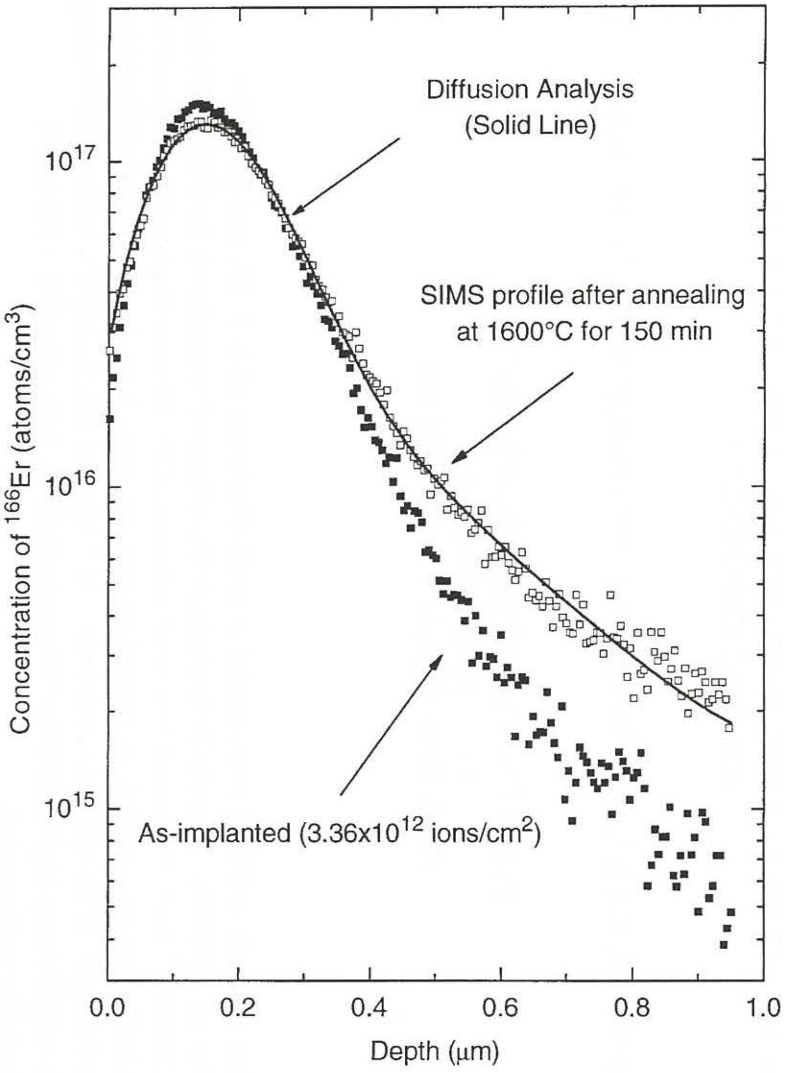

Figure 6. Depth Profiles of ^{166}Er As-Implanted in Polycrystalline UO_2 at 1230 keV to a Fluence of $3.36x10^{12}$ ions/cm^2 and After Thermal Annealing at 1600°C for 150 min. The Solid Line Depicts the Calculated Distribution (See Text).